EBioMedicine 56 (2020) 102782

Contents lists available at ScienceDirect

EBioMedicine

journal homepage: www.elsevier.com/locate/ebiom

Research paper

CD24-targeted fluorescence imaging in patient-derived xenograft models of high-grade serous ovarian carcinoma

Katrin Kleinmanns[a,1], Katharina Bischof[a,b,1], Shamundeeswari Anandan[a,b], Mihaela Popa[a,c], Lars A. Akslen[d], Vibeke Fosse[a,e], Ida Tveit Karlsen[a], Bjørn T. Gjertsen[a,f], Line Bjørge[a,b], Emmet McCormack[a,*]

[a] Centre for Cancer Biomarkers, CCBIO, Department of Clinical Science, University of Bergen, Jonas Lies vei 91B, 5021 Bergen, Norway
[b] Department of Obstetrics and Gynecology, Haukeland University Hospital, 5021, Bergen, Norway
[c] KinN Therapeutics, Jonas Lies vei 91B, 5021, Bergen, Norway
[d] Centre for Cancer Biomarkers, CCBIO, Department of Clinical Medicine, Section for Pathology, University of Bergen, Jonas Lies vei 87, 5020, Bergen, Norway
[e] Department of Radiology, Erasmus Medical Centre, 3000 CA Rotterdam, the Netherlands
[f] Department of Internal Medicine, Hematology Section, Haukeland University Hospital, 5021, Bergen, Norway

ARTICLE INFO

Article History:
Received 30 October 2019
Revised 2 April 2020
Accepted 21 April 2020
Available online xxx

Keywords:
Optical imaging
Fluorescence imaging
HGSOC
PDX
Biomarker
High-grade serous ovarian cancer
CD24

ABSTRACT

Background: The survival rate of patients with advanced high-grade serous ovarian carcinoma (HGSOC) remains disappointing. Clinically translatable orthotopic cell line xenograft models and patient-derived xenografts (PDXs) may aid the implementation of more personalised treatment approaches. Although orthotopic PDX reflecting heterogeneous molecular subtypes are considered the most relevant preclinical models, their use in therapeutic development is limited by lack of appropriate imaging modalities.
Methods: We developed novel orthotopic xenograft and PDX models for HGSOC, and applied a near-infrared fluorescently labelled monoclonal antibody targeting the cell surface antigen CD24 for non-invasive molecular imaging of epithelial ovarian cancer. CD24-Alexa Fluor 680 fluorescence imaging was compared to bioluminescence imaging in three orthotopic cell line xenograft models of ovarian cancer (OV-90^{luc+}, Skov-3^{luc+} and Caov-3^{luc+}, n = 3 per model). The application of fluorescence imaging to assess treatment efficacy was performed in carboplatin-paclitaxel treated orthotopic OV-90 xenografts (n = 10), before the probe was evaluated to detect disease progression in heterogenous PDX models (n = 7).
Findings: Application of the near-infrared probe, CD24-AF680, enabled both spatio-temporal visualisation of tumour development, and longitudinal therapy monitoring of orthotopic xenografts. Notably, CD24-AF680 facilitated imaging of multiple PDX models representing different histological subtypes of the disease.
Interpretation: The combined implementation of CD24-AF680 and orthotopic PDX models creates a state-of-the-art preclinical platform which will impact the identification and validation of new targeted therapies, fluorescence image-guided surgery, and ultimately the outcome for HGSOC patients.
Funding: This study was supported by the H2020 program MSCA-ITN [675743], Helse Vest RHF, and Helse Bergen HF [911809, 911852, 912171, 240222, HV1269], as well as by The Norwegian Cancer Society [182735], and The Research Council of Norway through its Centers of excellence funding scheme [223250, 262652].

1. Introduction

Epithelial ovarian carcinoma (EOC) remains the deadliest of all gynaecological malignancies in developed countries, with high-grade serous ovarian carcinoma (HGSOC) being the most common subtype [1]. The five-year survival rate is still below 50%, primarily attributed to late stage diagnosis and chemoresistance [2]. Cytoreductive surgery represents the main therapeutic option for the majority of patients, and complete tumour resection is a critical prognostic parameter for disease outcome [3,4]. Additional treatment approaches for HGSOC include platinum-based chemotherapy, and increasingly, precision therapeutics (*e.g.* VEGF- and PARP-inhibitors) targeting biological characteristics of the tumour, such as angiogenesis and defective homologous recombination DNA repair [5]. These novel classes of targeted drugs are fuelling hope of favourably changing the poor outcome for EOC patients [6,7]. The exploitation of

* Corresponding author.
E-mail address: emmet.mc.cormack@uib.no (E. McCormack).
[1] These authors contributed equally to this work.

https://doi.org/10.1016/j.ebiom.2020.102782

Research in Context

Evidence before this study

Patient-derived xenograft (PDX) models, incorporating inter-patient and intra-tumour heterogeneity, are considered clinically relevant animal models in prediction of patient outcome, drug response and treatment efficacy. However, preclinical PDX studies predominately employ subcutaneous engrafted tumour models for exploring therapeutic concepts, which has limited translational relevance. Orthotopic implantation of primary material into the physiological environment of the murine ovary permits metastatic spread and formation of malignant ascitic fluid, better reflecting the patient's disease course and clinical characteristics. Despite their superior clinical relevance, a major limitation in application and translation of preclinical concepts derived from orthotopic PDX models lies in disease staging and subsequent determination of intervention point. Thus, true exploitation of the translational power of orthotopic PDX models demands development of relevant imaging methodologies to quantify disease progression and therapeutic efficacy.

Added value of this study

In this study, we have developed novel orthotopic epithelial ovarian cancer patient-derived xenograft models, which reflects clinical disease progression and dissemination. To overcome the limited ability to monitor disease progression in these models, we have developed a non-invasive imaging approach using the EOC tumour-specific biomarker CD24. We demonstrate that CD24-targeted near-infrared fluorescence imaging allows visualisation of disease progression, identification of distant metastasis and the evaluation of treatment efficacy in orthotopic cell line and clinically relevant PDX models. Therefore, the presented methodology provides a new tool for preclinical evaluation of disease progression, development of new therapeutic regimes and precision therapy in the most clinically relevant modelling system of HGSOC, namely PDX.

Implications of all the available evidence

Our study demonstrates that CD24-targeted near-infrared fluorescence imaging of orthotopic PDX models of ovarian cancer can aid the development and evaluation of novel therapeutic drugs for ovarian cancer patients. PDX biobanks and the ability to monitor disease progression in heterogenous models with non-invasive imaging may further aid personalised medicine allowing the examination of a variety of drugs, identifying the most potent for each individual patient. CD24, a cancer stem cell marker, involved in tumour metastasis, represents a biomarker, which is highly expressed not only in ovarian carcinoma but also on several other tumours, and low in healthy tissue. This emphasises CD24 not only as a biomarker for optical near-infrared imaging in preclinical models but also a target for therapeutic approaches, as well as a potential biomarker for image-guided surgery.

tumour specific and sensitive biomarkers represents a safe and non-invasive imaging modality to detect tumour progression and response to treatment. Imaging biomarkers VEGF and HER2 [8,9], FRα [10], Thomsen-Friedenreich glycan antigen [11] and EpCAM [12] for the detection of metastasised carcinomas have all shown potential in preclinical xenograft drug efficiency studies, as targeted therapeutics and potential targets to improve surgical resections in the intraoperative setting [13,14].

Development and exploitation of novel tumour-specific theranostic biomarkers necessitates predictive preclinical models facilitating clinical translation. Ideally, preclinical systems should model cancer evolution as an interplay between neoplastically transformed, immortalised cells and the surrounding and systemic environment [15,16]. Genetically engineered models would initially appear ideal; however, these models lack the disease heterogeneity observed clinically while mouse homologues of human biomarkers often lack cross-reactivity [17,18]. Thus, human xenograft models better satisfy the conditions required for clinical translation of human imaging biomarkers [19]. However, recent landmark papers have revealed that commonly used HGSOC cell lines are not fully representative of the human paradigm, many of which have lost key molecular traits of the original samples [20,21]. Coupled with the frequent xenografting of these cell lines subcutaneously or intraperitoneally - neither of which replicates clinical conditions - necessitates more relevant models to improve clinical translation. Patient-derived xenografts (PDXs) represent a step towards optimal disease modelling as they are known to preserve the genetic landscape, phenotypic traits, including intra-tumour heterogeneity, and to predict response to therapy of the primary patient sample [22-25]. As such, orthotopic implantation of patient-derived material into immunocompromised mice appears to offer the most relevant context for therapy development in HGSOC [26,27], whilst also facilitating monitoring of tumour progression and treatment response in preclinical drug efficacy studies [28].

Typically, preclinical imaging to monitor the spatio-temporal development of disease, or therapeutic effects of novel agents *in vivo,* relies heavily on bioluminescence imaging (BLI) and/or PET/CT [29,30]. Nevertheless, BLI requires genetic alteration of the human cells to facilitate reporter gene expression, in addition to selection or sorting of expressing cells [30-32]. In the context of imaging PDX models, application of reporter gene strategies may be detrimental to the complex genetic traits and clonal heterogeneities prevalent in primary patient material. Furthermore, the development of haemorrhagic ascites, typical in orthotopic HGSOC PDX, abrogates BLI approaches owing to absorption of visible photons by haemoglobin, while PET/CT strategies are expensive and low throughput [33,34]. Therefore, alternative approaches for non-invasive preclinical imaging, particularly of orthotopic PDX models, are desired. Fluorescence imaging (FLI) of ovarian PDX with application of exogenous near-infrared (NIR) imaging probes thus appears a particularly attractive concept, requiring no genetic manipulation, and potential clinical translatability to PET/CT or fluorescence image-guided surgery (FIGS) [35]. It has previously been demonstrated that the exploitation of clinical immunophenotyping identified receptor-targeted optical imaging probes, which could be employed in PDX imaging and subsequent therapeutic response [34,36].

The objective of this study was to elucidate novel imaging markers for detection and monitoring of orthotopic HGSOC preclinical models, in particular *de novo* heterogenous PDX models. Here, we describe the identification of the EOC cell surface biomarker, CD24, through screening of ovarian carcinoma cell lines and patient material, and its application as an imaging biomarker. The choice of Alexa Fluor 680 (AF680) as fluorescent conjugate for CD24 was based on its spectral characteristics matching detector range of most optical imaging systems. Furthermore, AF680 demonstrates superior quantum yield and molecular extinction coefficients over corresponding cyanine dyes and molecularly, contain less sulfonate groups resulting in lower background accumulation [37,38]. We show that the conjugate of the monoclonal antibody CD24 and the NIR fluorophore AF680 (CD24-AF680) have no effect on cell viability, and we demonstrate that the application of this imaging probe for HGSOC cell line xenografts leads to improved identification of intraperitoneal tumour manifestations. Furthermore, the CD24-targeted NIR probe could be used longitudinally to monitor disease progression and therapeutic

efficacy in HGSOC xenografts and image EOC PDX, including those with low CD24 expression. Finally, we illustrate the application of this probe in other CD24 expressing PDX models and postulate its translational potential as an EOC theranostic.

2. Materials and methods

2.1. Cell lines and reagents

The human ovarian carcinoma cell lines Caov-3 (cat# HTB-75, RRID: CVCL_0201), OV-90 (cat# CRL-11732, RRID: CVCL_3768), and SKOV-3 (cat# HTB-77, RRID: CVCL_0532) were purchased from the American Type Culture Collection (ATCC, Manassas, VA, USA) and the COV318 (cat# 07071903, RRID: CVCL_2419) cell line was purchased through Sigma Aldrich (St. Louis, MI, USA). OV-90 cells were cultivated in RPMI 1640 and SKOV-3, Caov-3, and COV318 cells in Dulbecco's modified Eagle's medium (DMEM), supplemented with 10% heat-inactivated foetal bovine serum and 2 mM L-glutamine at 37 °C and 5% CO_2.

2.2. Retroviral transduction of cell lines

We engineered clones that stably express the light-emitting enzyme luciferase for the cell lines used, denoted Caov-3^{luc+}, OV-90^{luc+}, SKOV-3^{luc+}and COV318^{luc+}. In order to achieve stable expression of luciferase, we used the construct L192 for the OV-90^{luc+}, Caov-3^{luc+} and SKOV-3^{luc+}cell lines and the RediFect Red-FLuc-GFP lentiviral particles (cat # CLS960003, Perkin Elmer, Inc., Waltham, MA, USA) for COV318 both coding for the firefly luciferase enzyme. Infectious viral particles were harvested after 24 h of incubation. Retroviral infection was performed as described earlier [39] and according to the manufactures protocol.

2.3. Flow cytometry analysis

Cells were detached from the culture flask using Trypsin (cat # T3924-500, Sigma Aldrich), washed twice and a total of 5×10^5 cells of the Caov-3^{luc+}, OV-90^{luc+}, SKOV-3^{luc+}, and COV318^{luc+} cell lines were resuspended in 50 μL PBS (Dulbecco's tablets, cat # P4417-100TAB, Sigma Aldrich) supplemented with 1% solution of bovine serum albumin (BSA) (cat # 05482−100 G, Sigma Aldrich). Samples were incubated on ice for 30 min with one of the following monoclonal antibodies (mAb); EpCAM-PE (clone EBA-1, cat # 347198, RRID: AB_400262, BD Biosciences, Franklin Lakes, NJ, USA), CD24-PE (clone SN3, cat # LS-C46459-100, RRID: AB_1053866, LS Bio, Seattle, WA, USA), CD44-PE (clone 7F1, cat # LS-C46494, RRID: AB_2074685, LS Bio), FOLR1-PE (clone 548908, cat # FAB5646P, RRID: AB_10572835, RD systems, Minneapolis, MN, USA), and TAG72-PE (clone B72.3, cat # NBP2-52672PE, Novusbio, Littleton, CO, USA). Stained cells were washed with 1% BSA/PBS and resuspended in PBS before cells were acquired and recorded on a BD Accuri C6 or a BD Fortessa Flow Cytometer (both BD Biosciences, Franklin Lakes, NJ, USA) in 3 replicates.

2.4. Conjugation of antibody

A monoclonal, purified mouse-derived antibody directed against CD24 (clone SN3, cat # MCA1379, RRID: AB_321526, Bio-Rad, Oxfordshire, UK) was conjugated to the near-infrared dye Alexa Fluor 680 using the SAIVI Rapid Antibody Labelling Kit (cat # S30045, Invitrogen, Carlsbad, CA, USA) and purified by size exclusion chromatography, as described by the manufacturers. The resulting protein's (CD24-AF680) spectral characteristics were determined by Spark 20 M (Tecan, Männendorf, Switzerland, $\lambda_{absorbance}$ max 678 nm $\lambda_{fluorescence}$ max 706 nm) and protein concentrations were determined with a Nanodrop 1000 spectrophotometer (Fisher Scientific, Waltham, MA, USA).

2.5. Cell viability and apoptosis assay of CD24-AF680 in vitro

Toxicity and proliferation of Caov-3^{luc+}, OV-90^{luc+}, SKOV-3^{luc+}, and COV318^{luc+} cells after incubation with CD24-AF680 were evaluated. To validate the cell proliferation, cells incubated with CD24-AF680 and controls without mAb were compared using the cell proliferation reagent WST-1 (cat # 5015944001, Roche Applied Science, Pensberg, Germany). According to the manufactures protocol, 2×10^4 cells were incubated for 24, 48 or 72 h with or without CD24 (4 μg; 0.04 mg/mL) in triplicates before 10 μl of WST-1 reagent was added to the aliquots (90 μl). The formazan concentration was measured after four hours (Tecan Infinite 200 microplate reader and Magellan Version 6 Software; Tecan Trading, Maennedorf, Switzerland). All samples were normalised by the average of the 24-hour control triplet of each cell line. Apoptosis was assessed by extracellular phosphatidyl serine staining combined with propidium iodide (PI) (Alexa Fluor 488 annexin V/ Dead cell Apoptosis Kit for Flow cytometry, cat # V13242, Thermofisher). The staining was performed according to the manufacturer's manual. In short, 1×10^5 cells of each cell line were cultured in a six wells-plate and incubated for 24 or 48 h with CD24 mAb (4 μg). After incubation, control and treated cells were detached from the culture plates with trypsin, centrifuged and stained with 5 μL Alexa Fluor 488 Annexin V and 1 μL 100 μg/mL PI in 60 μL cell suspension for 15 min and analysed by flow cytometry (BD LSR Fortessa).

2.6. Patient characteristics and tissue processing

Tumour material was collected from a total of 30 women, who were diagnosed with and treated for EOC at Haukeland University Hospital, Bergen, Norway. Clinicopathological variables of the patient cohort are listed in Table 1. The local ethics committee approved the study and the biological samples were provided from the gynaecologic Cancer Biobank, Women's Clinic, Haukeland University Hospital,

Table 1
Clinicopathological variables patients (n = 30).

Clinical parameters Total number of patients (n = 30)	Median (range)
Age at diagnosis (years)	66 (28−83)
Follow-up time (months)	20 (1−62)
Progression-free interval (months)	16 (0−40)
Histological diagnosis	**N** (%)
HGSOC	22 (73·3)
Mucinous carcinoma of the ovary	1 (3·3)
Clear cell carcinoma of the ovary	2 (6·7)
Low-grade serous carcinoma of the ovary	2 (6·7)
Endometroid carcinoma of the ovary	2 (6·7)
Anaplastic carcinoma	1 (3·3)
FIGO 2014 stage	**N (%)**
IA	4 (13·3)
IC	3 (10)
IIA	1 (3·3)
IIB	4 (13·3)
IIIA	1 (3·3)
IIIC	13 (43·3)
IV	4 (13·3)
Level of surgical cytoreduction	
Complete	16 (53·3)
Residual disease at the end of surgery	14 (46·7)
(Neo)adjuvant chemotherapy	
Yes	7 (23·3)
No	23 (76·7)

Clinical characteristics (age at primary treatment, follow-up time and progression-free survival [PFS], histological subtype of epithelial ovarian carcinoma, FIGO 2014 stage, level of complete cytoreduction during primary surgery and chemotherapy status at time of sample collection) were collected from tumour samples acquired from hysterectomy specimens or diagnostic biopsies. PFS was defined as time in months from the first day of primary treatment to disease recurrence.

Bergen, Norway (REK ID: 2014/1907, 2015/548, 2018/72). Written informed consent was prospectively obtained from all women before collection of fresh frozen tumour tissue and clinicopathological parameters were initiated. After selecting non-necrotic tumour samples at a minimum size of 2 cm^3, tissue was immediately processed. Tumours were mechanically dissociated using two microscopic slides until a homogenous cell suspension could be filtered through a 40 μm cell strainer (cat # 732−2757, Corning Inc., USA). A part of the patient samples was additionally treated with Collagenase II (300 U/mL, cat # 17101015, Gibco, Paisley, UK) supplemented with the activity stabilizer $CaCl_2$ and TrypLE (cat # 12604013, Gibco, Paisley, UK). Cell suspensions were centrifuged at 350 g for five minutes, washed twice with PBS and cell concentrations were determined using a haematocytometer. Samples were stored in freezing medium (containing a final 10% DMSO 90% FBS) in liquid nitrogen or immediately injected into immunodeficient mice. Routine histopathological analysis of implanted material was performed at the Haukeland University Hospital, Department of Pathology, Bergen, Norway by experienced pathologists. Xenograft tissue specimens were fixed in buffered formalin and further processed before histological sections (4 μm) were made. Subsequently, slides were stained with Hematoxylin & Eosin (H&E) for assessment of morphology and immunohistochemistry for expression of CD24. Details of patients with corresponding engrafted PDX are listed in Table 2.

2.7. In vivo *xenograft models of ovarian cancer*

Animal experiments were performed in accordance with the procedures from the Norwegian Commission for Laboratory Animals, the European Convention for the Protection of Vertebrates Used for Scientific Purposes (EU Directive 2010/63/EU for animal experiments) and the ethical standards given in the Declaration of Helsinki of 2008, and approved by the Norwegian Food Safety Authority (Application IDs 8066 and 14128). Six to eight-week-old female NOD-*scid* IL2rγ^{null} (NSG) mice (weight 22 - 28 g) were housed at the University of Bergen's animal facility under defined flora conditions in individually ventilated (HEPA-filtered air) cages. No more than five mice were housed in each individually ventilated cage, which was kept on a 12-hour dark/night schedule at a constant temperature of 21 °C and at 50% relative humidity. Bedding and cages were autoclaved and changed twice per month, and the mice were weighed twice weekly. The animals had a continuous supply of sterile water and an irradiated low auto-fluorescence rodent imaging diet (D1001, Research diets, Brunswick, USA). Animals were monitored daily and sacrificed following institutional guidelines, as defined by weight loss >10%, or in case of ascites, distended abdomen, paleness, ruffled fur or lethargy. The post-mortem examination included macroscopic description of the primary tumour, presence and extent of metastases and ascitic fluid. Organs were removed, and bioluminescence and fluorescence imaging were performed on explanted organs. Collected tissue biopsies were fixed in 4% formaldehyde for 24 h, then washed in ddH2O and transferred to 70% EtOH for long-term storage.

Ovarian carcinoma cell lines (OV-90^{luc+}, SKOV-3^{luc+}, and Caov-3^{luc+}) and patient-derived single cell suspensions, resuspended in PBS, were xenografted either orthotopically or subcutaneously. Anaesthetic and operative procedures for orthotopic xenograft models on mice were performed as described previously [19]. For subcutaneous models, 5×10^6 human tumour cells suspended in PBS were mixed 1:1 with Matrigel membrane matrix (cat # 10365602, Corning Inc, USA) to a final volume of 100 μL. Cell suspensions were injected bilaterally into the flanks of female NSG mice after depilation and disinfection with chlorhexidine 5 mg/mL (Fresenius Kabi, Halden, Norway).

Table 2
CD24 expression profiles of patients included (n = 30).

Patient ID	Tumour engraftment	CD24 status	CD24 SI (continuous)	Histology
1	yes	1	4	HGSOC
2	yes	1	9	HGSOC
3	yes	1	9	HGSOC
4	yes	1	9	HGSOC
5	yes	1	6	HGSOC
6	yes	1	4	clear cell
7	yes	0	0	anaplastic
8	no	1	9	HGSOC
9	no	0	0	endometroid
10	no	1	3	endometroid
11	no	1	4	HGSOC
12	no	0	0	HGSOC
13	no	1	6	HGSOC
14	no	1	6	HGSOC
15	no	1	9	HGSOC
16	no	1	3	HGSOC
17	no	1	1	HGSOC
18	no	1	3	LGSOC
19	no	1	4	clear cell
20	no	1	6	HGSOC
21	no	1	2	HGSOC
22	no	1	6	HGSOC
23	no	/	/	LGSOC
24	no	1	4	HGSOC
25	yes (P0)	1	4	HGSOC
26	no	1	4	HGSOC
27	no	1	9	HGSOC
28	yes (P0)	1	4	HGSOC
29	yes (P0)	1	4	HGSOC
30	yes (P0)	1	3	mucinous

Successful tumour engraftment yes (passage; $P > 0$, $P = 0$) or no; CD24 status expressed as positive = 1 or negative = 0; SI = immunohistochemical staining index calculated from CD24 staining intensity (0−3) x positive stained area (0−3); 0 = no expression, 9 = strong expression; HGSOC = high-grade serous ovarian carcinoma; LGSOC = low grade serous ovarian carcinoma.

2.8. Optical imaging

Mice were fed a low auto-fluorescence rodent imaging diet (cat # D1001, Research diets Inc., Brunswick, USA) for at least one week prior to imaging experiments. The mice were anaesthetised as described above and depilated before near infrared (NIR) images were obtained with the Optix MX3 Small Animal Molecular Imaging system (ART Inc. Saint Laurent, QC, Canada) or the IVIS Spectrum *In Vivo* Imaging System (Perkin Elmer). Fluorescence imaging (FLI) scans (MX3 λ_{ex} = 670 nm, λ_{em} = 700 nm LP, laser repetition rate 80 MHz, raster scan points 1 mm apart; IVIS 684 ± 15 nm excitation bandpass filter and 702 ± 10 nm emission bandpass filter) were obtained 24 h after administration (or as otherwise indicated) of CD24-AF680 (total mAb concentration of 2 μg/g body weight) [36]. The purified mouse IgG1 antibody (cat # MCA928EL,RRID:AB_324,168, Bio-Rad) conjugated to Alexa Fluor 680 was used as a negative control. For bioluminescence imaging (BLI), bioluminescent signal was acquired 10 min after the administration of D-luciferin (150 mg/kg, cat # L-8220, Biosynth, Staad, Switzerland). FLI and BLI of xenograft mice was performed weekly. During early disease stages or minimal tumour burden post-treatment, mice were imaged in the lateral view, to allow for detection of small tumour deposits, whereas the ventral view was used for visualisation of metastatic disease dissemination in the peritoneal cavity. All images and fluorescence lifetime gating (Supplementary fig. S1) were analysed with OptiView software (Version 2.02; ART Inc) and/or Living image software (Perkin Elmer) [40,41]. Background fluorescence signal, identified by fluorescence lifetime gating (Supplementary fig. S1), was gated out from all the resulting FLI images (OptiView software Version 2.02; ART Inc).

2.9. Evaluation of CD24-AF680 imaging in treated OV-90 orthotopic xenograft models

NSG mice (n = 10) were implanted orthotopically with 2×10^4 OV-90^{luc+} cells. Following the establishment of the primary tumour, defined as the first FLI acquired signal at the primary injection site, mice were randomised based on FLI signal intensity, and grouped into two cohorts, vehicle control (n = 4) and treatment group (n = 6). The treatment group received Paclitaxel (15 mg/kg; Fresenius Kabi, Halden, Norway 6 mg/mL) and Carboplatin (12 mg/kg; Fresenius Kabi, Halden, Norway 10 mg/mL) Q2Wx3. One day before the first treatment and one week after the final treatment dose, all mice were imaged laterally and ventrally by BLI and FLI as described above (Optical imaging). All animals were sacrificed thereafter and disease burden, tumour weights and *ex vivo* fluorescence intensities were evaluated.

2.10. Intraoperative fluorescence imaging

The potential clinical application of CD24-AF680 as a tracer for fluorescence image-guided surgery was investigated using the FLARE® intraoperative NIR fluorescence imaging system (Curadel LLC, Marlborough, USA). Orthotopic OV-90^{luc+}and one PDX model were anaesthetised as described, and a midline coeliotomy was performed. Intraoperative images were captured using the NIR 700 channel, λ_{ex} = 665 ± 3 nm and λ_{em}710 ± 25 nm bandpass filters, at an exposure time of 500 - 1500 ms and gain of 1. The colour video channel with an illumination source of 400 - 660 nm and the NIR 700 channel were simultaneously acquired and overlaid to a pseudo-coloured merge image in real-time. The imaging head was attached to moveable arm, allowing a 24•5 cm working distance with a field of view of 7•7 cm^2. The mice were sacrificed at the end of the procedure.

2.11. Histology and immunohistochemistry

Immunohistochemical (IHC) staining was done on formalin-fixed and paraffin-embedded (FFPE) ovarian tumour tissues sectioned at 4 μm thickness. After de-paraffinization in xylene and rehydration through graded ethanol series and distilled water solutions, the tissues were subjected to heat-induced epitope retrieval undertaken in TRS citrate buffer (pH=6.0) (cat # S1699, Agilent Technologies, Norway) by the use of a microwave oven (Whirlpool, JT366; Expert Bonus, Norway) for 20 min. After antigen retrieval, tissues were incubated for 8 min with peroxidase blocker (Peroxidase Blocking Reagent, cat #S2001, Agilent Technologies) and thereafter for 10 min with protein blocker (Protein Block Serum-free, cat # X090930-2, DAKO, Copenhagen, Denmark) at room temperature. The blocking solution was then removed and the slide was wiped dry around the tissue section before application of the primary antibody. The sections were then incubated overnight at 4C degrees with the CD24 primary antibody (clone SN3b, cat #MA5-11,833, RRID:AB_10,985,938 Thermo Fisher Scientific) dilution 1:25. The staining was performed on a DAKO Autostainer using the EnVision+ System-HRP Labelled Polymer Anti-Mouse K4001 as secondary antibody for 30 min (Agilent Technologies, Norway). 3,3`-Diaminobenzine (DAB+) Substrate-Chromogen was used as chromogen for 10 min. Sections were counterstained with haematoxylin (cat # S3301, Agilent Technologies) for 10 min, dehydrated, and mounted with a coverslipper (Agilent Technologies) using Pertexx mounting medium (Histolab Products AB, Askim, Sweden). Negative control sections underwent the same procedure but without including the primary antibody. Human tissue from high-grade serous ovarian carcinoma with known reactivity to the selected marker was used as positive control, and physiological ovarian tissue from a healthy mouse of the same breed and age was used as negative control. The CD24 staining indices for the patients included are listed in Table 2. CD24 membrane expression by immunohistochemistry was determined by a staining index (SI; range 0–9), representing the product of intensity (0–3; negative, weak, moderate, strong; and area fraction of the tumour cells stained, 1–3; 1 = ⟨10%; 2 = 10–50%; 3 = ⟩ 50%). Cytoplasmic staining was observed in some cases, also in benign tissues, but was not recorded.

2.12. Statistical methods

The association between categorical variables in patients, such as CD24 expression status and tumour resectability or relapse status, were evaluated using the Pearson Chi-square test. When correlating non-binary variables, such as CD24 staining index, proliferation, apoptosis, FIGO stage, histological subtype or fluorescence intensity, with categorical variables for treatment outcome, the Mann-Whitney U test was applied. Survival analyses were performed by the Kaplan-Meier method, and subsets of patients were compared using the log-rank test. All p-values are two tailed, and p-values $<$ 0•05 were considered significant. Plot values are represented as mean ± standard deviation. Statistical analyses were performed using the software package SPSS 24.0 (SPSS Inc., Chicago, IL, United States of America) and GraphPad Prism (GraphPad Software Inc, San Diego, CA).

3. Results

3.1. Immunophenotyping of ovarian carcinoma cells and safety evaluation of CD24 monoclonal antibody

We hypothesised that fluorescently labelled monoclonal antibodies (mAbs), targeting highly expressed HGSOC antigens would allow the specific non-invasive detection of ovarian cancer xenografts *in vivo*. We screened a panel of EOC cell lines (OV-90^{luc+}, Caov-3^{luc+}, SKOV-3^{luc+}, and COV318^{luc+}) for expression of putative biomarkers (human-CD24, EpCAM, FolR1, CD44, and TAG72) by flow cytometry (Fig. 1a) and identified CD24 as overall homogeneously, highly expressed cell surface marker. CD24 expression was additionally evaluated by IHC in a cohort of tumour samples from 30 patients with EOC, of which almost 90% (26) stained positive for CD24, 10% (3) were negative, and one patient could not be analysed (Table 2). To determine whether the mouse anti-human CD24 mAb would have any effect on cell proliferation or viability, all cell lines were incubated with hu-CD24 for 24 to 72 h and proliferation assayed by WST-1 and viability by Annexin V/PI assay (Fig. 1b and 1c). No significant effects upon cell proliferation (Fig. 1b; p > 0•05) or cell viability (Fig. 1c; p > 0•05) were noted.

3.2. In vivo *CD24-AF680 identifies tumour lesions in epithelial ovarian carcinoma cell line xenografts*

To assess the sensitivity and specificity of CD24 as tumour-specific target *in vivo*, the NIR fluorophore AF680 was conjugated to the mouse anti-human CD24 mAb (as described in materials and methods). The biodistribution of CD24-AF680 and IgG1-AF680 was evaluated in orthotopic xenograft models by dynamic imaging every 24 h for five consecutive days (Supplementary fig. S2a). Non-invasive fluorescence imaging indicated a long circulation time of CD24-AF680 with the highest signal intensity and tumour to background ratios after 24 h similar to previous results with IgG conjugated mAbs (Supplementary fig. S2a) [41-43]. To investigate CD24-specific accumulation in tumour tissues, we compared the fluorescence intensity of orthotopic tumours in xenograft models imaged with CD24-AF680 and IgG1-AF680 24 h after injection (Supplementary fig. S2b – S2e). *Ex vivo* fluorescence imaging of dissected organs indicates the biodistribution of the antibody-conjugate (Supplementary fig. 2b). Orthoptic and subcutaneous xenograft models imaged with CD24-AF680 revealed an increased fluorescence signal in the tumours compared

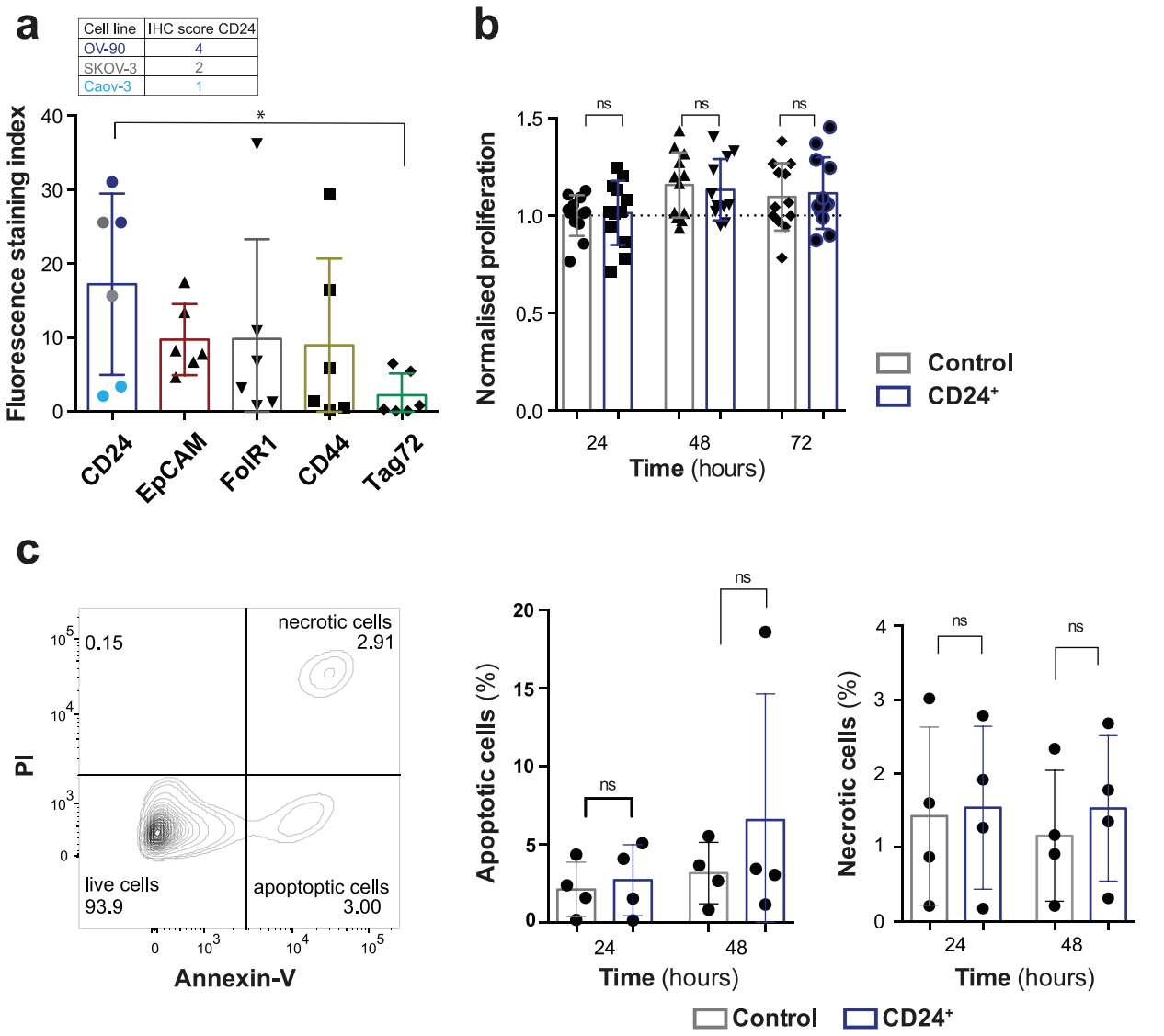

Fig. 1. Epithelial ovarian cancer biomarker screening and *in vitro* evaluation. (a) Flow cytometry-based analysis of stem cell marker expression profiles (CD24, EpCAM, FolR1, CD44 and Tag72) tested in three epithelial ovarian carcinoma cell lines (OV-90, Caov-3, and SKOV-3). The fluorescence staining index is based on the geometric mean fluorescence and normalised to the unstained control. (p = 0•026) The immunohistochemical staining index of CD24 (IHC, scale: negative 0 – 9 high) for all cell lines is indicated, correlating with the fluorescence signal intensity (b) WST-1 cell proliferation assay; cells were incubated for 24, 48, and 72 h in triplicates with and without CD24 monoclonal antibody (mAb). Proliferation in all cell lines was quantified using the WST-1 reagent, normalised to 24 h control ($p > 0$•05). (c) After incubating the EOC cell cultures (n = 4) with and without CD24 mAb for 24 and 48 h, potential toxicity and side effects of the mAb were quantified using the Annexin V/PI staining assay ($p > 0$•05). Each column represents the mean with SD and statistical analysis (Mann-Whitney U test) with $p < 0$•05 were regarded as statistically significant.

to the isotype control (Supplementary fig. S2b – S2f). In order to assess the general *in vivo* application of CD24-AF680 for EOC imaging, we employed the previously SKOV-3^{luc+} model [19], and generated two orthotopic xenograft models of HGSOC using OV-90^{luc+} and Caov-3^{luc+}cell lines, described here briefly.

Single suspensions of luciferase expressing cells (5×10^4 cells per mouse) were orthotopically injected into the bursa of recipient NSG mice (n = 5 per cell line) and mice were imaged weekly by BLI and FLI (Fig. 2a, Supplementary fig. S3a, S4a). For the OV-90^{luc+} and SKOV-3^{luc+} cell line models, a disease penetrance of 100% was observed, while the Caov-3^{luc+} cell line formed tumours that could be visualised by CD24-AF680 FLI and in *ex vivo* macroscopic examination in 40% of animals. Mean survival times of 43 ± 11 days (OV-90^{luc+}), 79 ± 20 days (SKOV-3^{luc+}), and 227 days (Caov-3^{luc+}) were noted for the individual models. OV-90^{luc+} and SKOV-3^{luc+} models were characterised by diffuse, intraperitoneal metastases after a minimum of three weeks (Fig. 2a and 2b, Supplementary fig. S4), while only one of the Caov-3^{luc+}implanted mice demonstrated metastatic spread (Supplementary fig. S3).

Cumulative analysis and comparison of both FLI and BLI optical imaging results from all three models (n = 3 mice per cell line) suggest superiority of the CD24-AF680 protocol. While both BLI and FLI permitted longitudinal monitoring of HGSOC disease dissemination, CD24-AF680 FLI imaging permitted earlier tumour detection, most evident in both Caov-3^{luc+} and SKOV-3^{luc+} models when compared with BLI (Supplementary fig. S3 and S4). CD24-AF680 permitted visualisation of superficial liver metastases in the OV-90^{luc+} model (Fig. 2a and 2b), as well as allowing visualisation of bilateral ovarian tumour masses in the Caov-3^{luc+} model, which were not evident in corresponding BLI imaging, but confirmed to be malignant and CD24 positive by IHC (Supplementary fig. S3a). Thus, signal intensities of fluorescence do not positively correlate with the total bioluminescence signal intensity (Fig. 2c). Similarly, evidence of metastases was apparent from CD24-AF680 FLI imaging of the SKOV-3^{luc+} model as

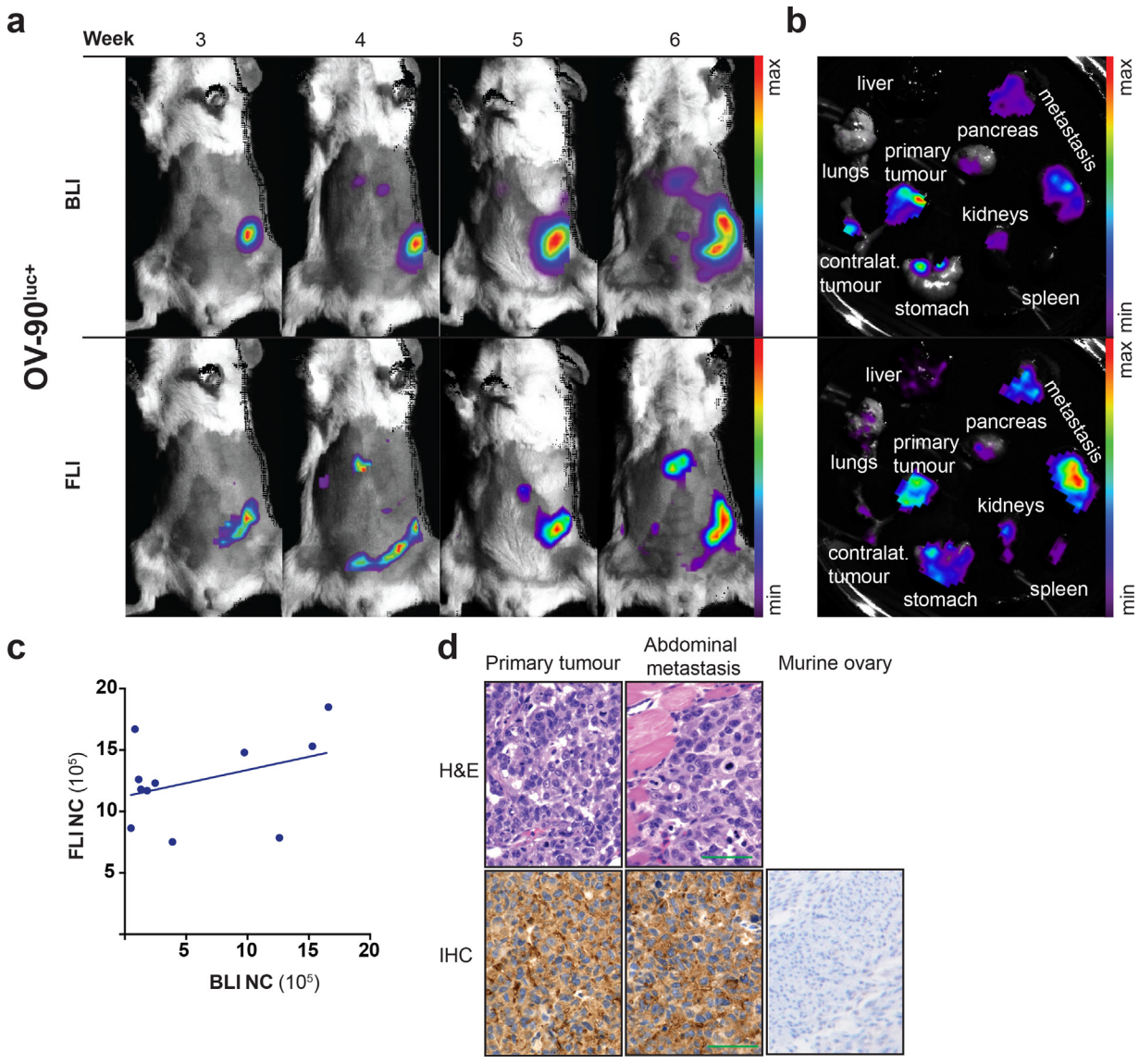

Fig. 2. *In vivo* optical imaging of OV-90^{luc+}xenograft models. (a) Comparison of longitudinal BLI and FLI imaging in orthotopic OV-90^{luc+}xenograft models (n = 3). CD24-AF680 fluorescence imaging, 24 h after probe injection, visualise the primary tumour and liver metastasis. (b) *Ex vivo* bioluminescence and fluorescence images demonstrate the tumour manifestation of one representative mouse. (c) Correlation of fluorescence to bioluminescence signal intensity measured in three individual mice over time (r^2 = 0•14). (d) H&E stained primary tumour tissue and abdominal metastasis and CD24 immunohistochemical staining of OV-90^{luc+}tumour tissues (staining index = 4, scale: negative 0 – 9 high) and murine ovarian tissue (negative); Scale bars: original magnification of x400 mm. All optical images are presented with the minimum to maximum fluorescence/bioluminescence intensity for each mouse and *ex vivo* organs. FLI = fluorescence imaging; BLI = bioluminescence imaging; NC = number of counts; IHC = Immunohistochemistry.

early as week six, whilst corresponding BLI imaging did not allow detection of metastases until four weeks later (Supplementary fig. S4a). *Ex vivo* imaging confirmed that HGSOC tumour tissue was detected with high specificity at both the primary injection site and as disseminated disease, with superficial spread on the mesenteric surface on the stomach, the intestine and the peritoneal lining of the abdominal wall (Fig. 2a and b, and Supplementary fig. S4a and S4b). The expression of the CD24 surface biomarker was confirmed on cell line xenografts *ex vivo* by IHC (Fig. 2d). Analysis revealed that tumours derived from implantation of OV-90^{luc+} and SKOV-3^{luc+} showed membranous CD24 expression with an immunohistochemical staining index (scale: negative = 0 – 9 = high) of four and two, respectively (Fig. 2d, Supplementary fig. S4d). For implants derived from xenografted Caov-3^{luc+}cells, we confirmed the bilateral tumour dissemination and identified low CD24 expression (staining index 1 - 2) in the primary tumour and uterus, thus supporting the specificity of CD24-AF680 (Supplementary fig. S3d and S3e).

3.3. CD24-AF680 enables reliable FLI monitoring of treatment efficacy

Given the observed sensitivity of CD24-AF680 for optical imaging of EOC xenografts, we addressed the utility of CD24-AF680 in a therapeutic setting with the OV-90^{luc+}xenograft model. OV-90^{luc+}xenografted mice (n = 10) were imaged weekly and upon tumour manifestation at the primary tumour site, as visualised by CD24-AF680, were randomised according to fluorescence intensity into two cohorts. One cohort was treated with a combination regime of 15 mg/kg paclitaxel and 12 mg/kg carboplatin twice weekly for 3 consecutive weeks, while the second served as vehicle control. CD24-AF680 imaging was performed immediately prior to and post therapy (Fig. 3a). Analysis of CD24-AF680 imaging of the control cohort (n = 4) illustrated progressive disease stages with visible metastases noted at distal sites such as the kidney, diaphragm, liver and stomach (Fig. 3a and 3c). Quantification of CD24-AF680 fluorescence revealed an almost 4-fold average increase in fluorescence intensity post-

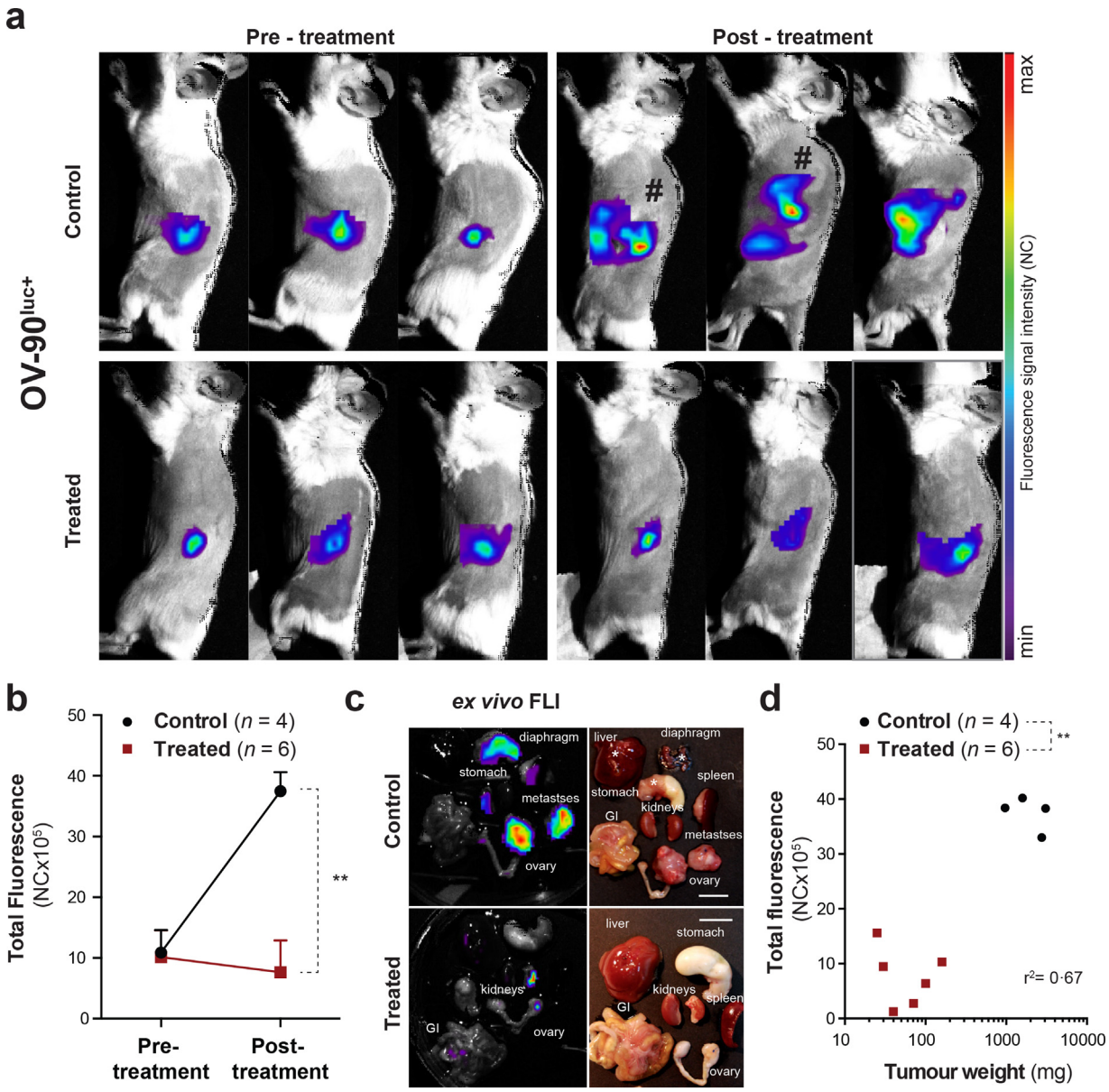

Fig. 3. CD24-FLI application study in orthotopic OV-90^{luc+}xenograft models. (a) Illustration of CD24-NIR fluorescence imaging in three representative OV-90^{luc+}orthotopic xenografted mice before and after treatment with chemotherapy (12 mg/kg carboplatin and 15 mg/kg paclitaxel [Q2Wx3]) and control. Mice marked with "#" are represented with higher maximum values. (b) The mean total fluorescence intensity before and after chemotherapy is illustrated for control and treated animals (n = 10, p = 0•0095). (c) *Ex vivo* fluorescence images and necropsy pictures (scale bar 1 cm) presenting (*-marked) tumour infiltrated organs and tumour progression in control *versus* treated mice. (d) Correlation of total fluorescence intensity and tumour load, represented as tumour weight (r^2 = 0•67) in control and treated mice (p = 0•0038). Data points represented as mean and SD. Statistical analysis (Mann-Whitney U test) with $p < 0•05$ (*), $p < 0•01$ (**) were regarded as statistically significant. FLI = fluorescence imaging; NC = number of counts; GI = gastrointestinal tract.

treatment (Fig. 3b; pre-treatment 10•90 × 10^5 ± 3•73 × 10^5 vs post-treatment 37•48 × 10^5 ± 3•11 × 10^5 [NC x 10^5]; $p < 0•03$). In contrast, CD24-AF680 imaging of the treated group revealed an average decrease in total fluorescence post therapy (pre-treatment 10•16 × 10^5 ± 4•4 × 10^5 vs post-treatment 7•63 × 10^5 ± 5•3 × 10^5 [NC x 10^5]) suggesting stable/reduced disease burden (Fig. 3B; $p > 0•05$). Comparison of CD24-AF680 FLI demonstrated therapeutic effect, with significant differences in total fluorescence exhibited between groups post-treatment (Fig. 3b; $p < 0•01$). All animals were euthanised post therapy, examined macroscopically, imaged and weighed. While *ex vivo* imaging confirmed the presence of metastases in the control cohort, both imaging and macroscopic examination confirmed that the disease was confined to visible primary tumours in the treated cohort (Fig. 3c). Finally, tumour weights of control and treated primary tumours confirmed CD24-AF680 imaging observations of significant differences following therapy (Fig. 3d; 71 ± 52 mg *vs*2098 ± 989 mg; $p < 0•01$, r^2 = 0•67) thus demonstrating the utility of CD24-AF680 FLI to accurately determine therapeutic effect non-invasively.

3.4. FLI of CD24-AF680 in patient-derived xenograft models

Having established the application of CD24-AF680 targeted FLI in longitudinal and therapeutic imaging of EOC cell lines, we wished to examine its utility for imaging heterogeneous PDX models of HGSOC by fluorescence as an approach to circumvent the transduction of primary material. Samples from 30 individual patient tumour tissues were collected at the time of primary surgery (patient characteristics Tables 1-3). After immediate tissue processing, single cell suspensions containing 1 × 10^4 to 5 × 10^4 patient-derived cells were

Table 3
Clinicopathological variables PDX models (n = 7).

Patient characteristics					PDX characteristic	CD24 status	
PDX	Age	Histology	FIGO	PFS (months)	Disease Latency (weeks)	Patient (SI)	PDX (SI)
1	52	HGSOC	IV	9	11	4	9
2	38	HGSOC	IIIC	40	19	9	9
3	75	HGSOC	IIIC	9	61	6	6
4	42	HGSOC	IIIC	13	16	9	4
5	64	HGSOC	IIA	2	13	6	6
6	78	Clear cell	IA	19	54	4	4
7	60	Anaplastic	IIIC	1	9	0	2

Clinical characteristics: Patient age at primary treatment, histological subtype of epithelial ovarian carcinoma, FIGO 2014 stage, progression-free survival (PFS), engraftment time in immunodeficient mice and CD24 expression status of the original patient material and the corresponding PDX sample indicated as immunohistochemical staining index (SI). SI = CD24 staining intensity (0–3) x positive stained area (0–3); 0 = no expression, 9 = strong expression. PFS was defined as time in months from the first day of primary treatment to disease recurrence.

injected into the left ovarian bursa or 5×10^6 cells were implanted subcutaneously into the flank of female NSG mice (n = 1 mouse per patient sample). Tumour engraftment was confirmed in 11 of 30 samples (overall engraftment of 37%), with seven (consisting of five HGSOC tumours, one anaplastic tumour, and one clear cell carcinoma) developing reproducible disease models (23%; Fig. 4, Supplementary fig. S5, Table 2 and 3). Time to engraftment was between 9 and 61 weeks and murine PDX development was associated with a significantly shorter time to clinical progression in the patient (log-rank test, p = 0•003; see Supplementary fig. S6). In all seven (100%) passaged PDX we confirmed CD24 expression by IHC and CD24 expression status was conserved in four of seven specimens (57%) (Fig. 4d and 4e, Supplementary fig. S5, Table 3). Interestingly, CD24 staining index increased in the two PDX models with the shortest overall engraftment time.

Initially, we examined the utility of CD24-AF680 FLI to visualise a subcutaneous HGSOC PDX model, and we demonstrated both fluorescent staining of *in vivo* tumours and a strong correlation (r^2 = 0•96) between tumour volume and CD24-AF680 fluorescence intensity (Fig. 4a). Next, we assessed CD24-AF680 FLI in orthotopic HGSOC PDX models (Fig. 4b). CD24-AF680 FLI revealed orthotopic tumour engraftment in the ovary and tumour dissemination in the peritoneal cavity, the stomach and omental tissue (Fig. 4b and 4c). *Ex vivo* examination and CD24-AF680 imaging demonstrated that fluorescence was detected in the ovaries and in peritoneal metastases, and metastatic spread was identified in the contralateral ovary, the peritoneum, liver, stomach, and diaphragm, similar to the disease progression observed in the patient counterpart (Fig. 4c and 4e). Human tumour origin and CD24 expression was confirmed in all HGSOC PDX models by H&E and IHC (Fig. 4d). To evaluate the relevance and sensitivity of CD24-AF680 FLI in longitudinal monitoring of HGSOC disease progression, we imaged one PDX model over its disease course, noting a linear increase in fluorescence over time (Fig. 4e). The data suggest the high potential of CD24-AF680 targeted FLI in all engrafted HGSOC PDXs with the ability to follow tumour progression. To demonstrate the versatility of CD24-AF680 FLI in imaging other $CD24^+$ PDX models, CD24-AF680 FLI was employed to visualise engraftment in a PDX model of clear cell carcinoma and anaplastic carcinoma (Supplementary fig. S5). Interestingly, while the primary patient sample of PDX7 was confirmed to be CD24 negative by IHC and of an anaplastic subtype, the PDX sample stained positive for CD24 with a staining index of two and an overall short engraftment time of nine weeks. While *in vivo* FLI imaging with CD24-AF680 of PDX7 revealed abdominal and liver metastases, primary *in vivo* tumour fluorescence was absent, and only possible to demonstrate *ex vivo*. This tumour was highly vascularised, suggesting that *in vivo* fluorescence was absorbed by haemoglobin (Supplementary fig. S5b).

Given the recent developments of tumour-targeted fluorescence image-guided surgery in ovarian cancer patients, there is a need for novel tumour-specific biomarkers which are not widely expressed in healthy tissues. Considering the applicability of CD24-AF680 for non-invasive fluorescence imaging, we investigated whether the probe also comprises potential for intraoperative image-guided surgery. In one orthotopic OV-90^{luc+} and one PDX model (n = 2), CD24-AF680 facilitated real-time, intraoperative detection of the primary tumour (Supplementary fig. S7a and S7b). In addition, ovarian metastatic tumour lesions in the spleen were identified (Supplementary fig. S7a). Autofluorescence from the stomach and gastrointestinal tract were observed at this wavelength (Supplementary fig. S7, green dashed lines).

4. Discussion

The cell surface marker CD24 has been shown to be significantly upregulated in a number of carcinomas compared to their benign counterparts, suggesting it as an ideal target for theranostic applications [44-46]. In our cohort of 30 cases of epithelial ovarian carcinoma we found expression of CD24 present in 90% of tissues, concurring with the observation that CD24 is highly expressed in the vast majority of ovarian cancer cases [47-49] with highest expression levels in the serous subtype [47,48,50,51]. Overdevest et al. reported higher CD24 staining indices in metastases and identified CD24 as the most overexpressed amongst transcripts in metastasising cells of human bladder carcinoma [52]. Numerous studies have associated CD24 expression on different tumour types with poor prognosis, tumour aggressiveness and positive correlation of CD24 expression to tumour growth, cell invasion and metastatic progression [45,51]. While we did not observe an association of CD24 expression with disease characteristics, resectability, FIGO stage or histological subtype in our clinical cohort of 30 patients, all seven PDX models derived from these samples demonstrated an aggressive clinical course, which might be explained by our highly selected patient series, which included clinically aggressive and mainly advanced tumours.

The results presented here may have broad applications for the modelling, detection and targeted treatment of advanced HGSOC. Translational and personalised therapy development is dependant on the fidelity of preclinical models that faithfully recapitulate the clinical paradigm [16]. Both the OV-90^{luc+} and Caov-3^{luc+} orthotopic models presented here are previously undescribed. These models accurately reflect the morphological characteristics, typical diffuse dissemination and ascites production throughout the peritoneal cavity observed clinically in HGSOC. Several reports have independently demonstrated that these cell lines result in greater molecular fidelity to HGSOC compared with the most commonly used cell line SKOV-$3^{luc+}$and we additionally demonstrate the efficacy of the orthotopic OV-90^{luc+} model in evaluation of clinical employed chemotherapeutics [20,21,53,54]. Coupled with the establishment of a panel of seven clinically annotated PDX models with patient FIGO stage II-IV, which

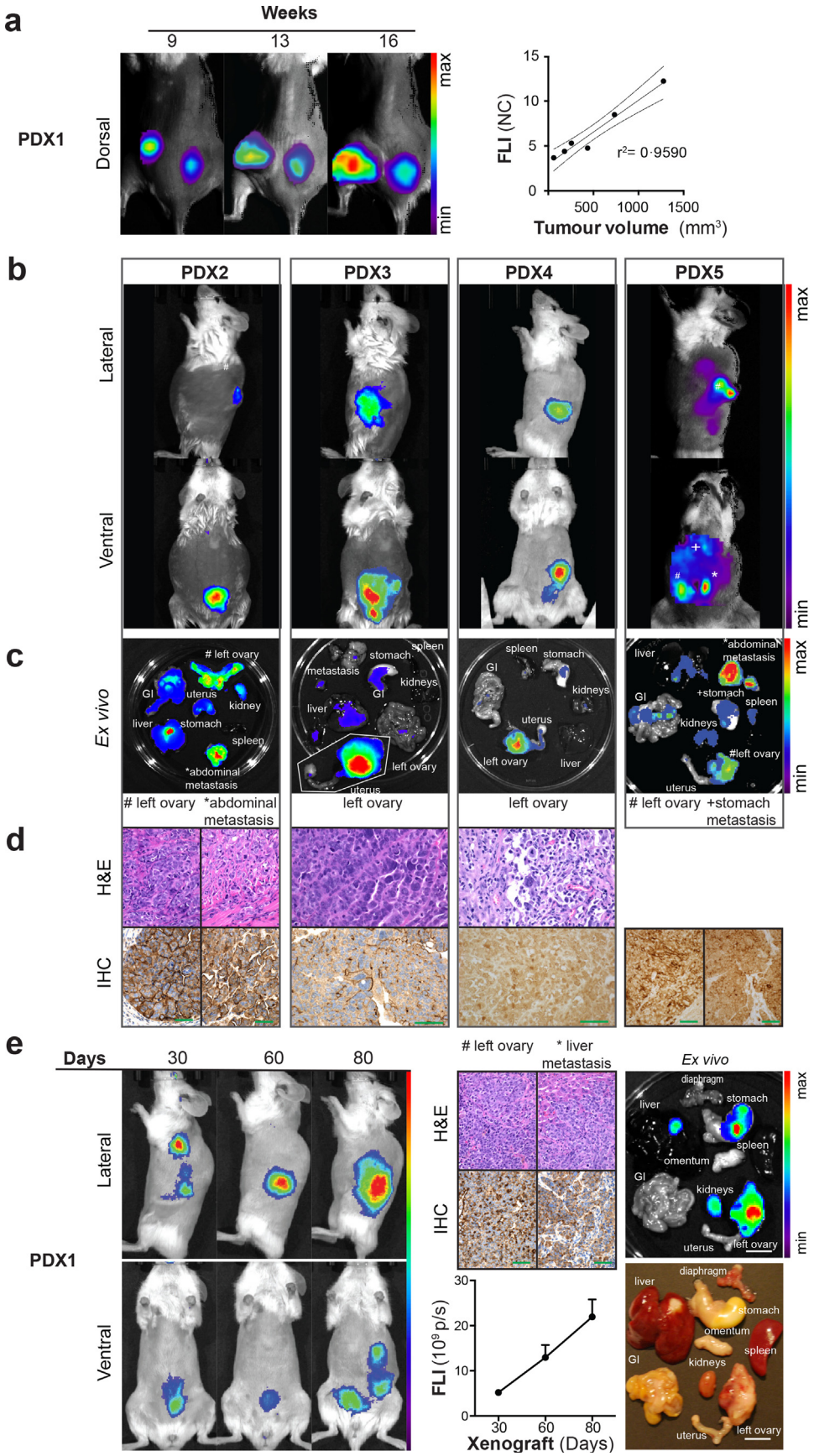

Fig. 4. Fluorescence imaging of high-grade serous ovarian cancer patient-derived xenograft (PDX) models using CD24-AF680. (a) Fluorescence imaging enables the detection of tumour progression in subcutaneous PDX models. Linear regression analysis showed correlation (r^2 = 0•96) of tumour size to fluorescence intensity. (b) Orthotopic implanted PDX models (n = 4) were imaged 24 h after CD24-AF680 injection (2 μg/g). Primary tumour lesions and metastases were detected by fluorescence optical imaging *in vivo* and (c) *ex vivo*. (d) Immunohistochemical (IHC) and H&E staining of the primary tumour and metastases confirmed CD24 expression and human tumour origin. Scale bars: original magnification

maintain similar histopathological features to the primary patient tumour, these models provide a crucial platform for therapy development in HGSOC. High throughput drug screening in genomically characterised PDXs showed 95% congruency with clinical response in several solid tumour types and is currently being evaluated in a phase II clinical trial (NCT02312245) for EOC [26,55,56].

Bioluminescence imaging is considered the gold standard of optical imaging, requiring the integration of reporter gene DNA into the chromosomes of the tumour cells [57]. This may inadvertently disrupt the delicate genomic landscape of primary patient material, and additionally becomes expensive in larger cohorts of PDX. In the current study we demonstrate the usefulness of CD24-AF680 FLI approach, particularly in early and metastatic detection in HGSOC preclinical models and we showed the ability to longitudinally follow disease progression in both cell line and PDX models using CD24-AF680, avoiding unnecessary genetic alteration of the cell genome. However, long circulation time of the monoclonal antibody suggests the further development of the probe into antibody fragments, such as nanobodies, diabodies or affibodies, with preferred biodistribution characteristics that would allow more frequent imaging [58,59]. Attempts to enhance tumour to background ratios on the one hand, and limited tissue penetration depth of fluorescence on the other, are further exploited by the development of activatable probes, longer wavelength shifted NIR I fluorophores (*e.g.* IRDye 800CW, ZW800-1) and synthetic nanoprobes labelled with NIR II fluorophores [60-62]. A caveat of non-invasive optical approaches is the limited sensitivity in highly vascularised and haemorrhagic environments, as demonstrated for PDX7. Numerous studies have highlighted the potential of CD24 as a therapeutic agent to reduce tumour growth, alter the intratumoural cytokine microenvironment, increase the infiltration of immune cells into the tumour tissue and investigate CD24 in adoptive immunotherapy [52,63,64]. Thus, evolution of our CD24-AF680 probe to incorporate a PET radionuclide such as ^{89}Zr or ^{64}Cu or SPECT probe ^{68}Ga or ^{111}In would generate a quantitative theranostic probe with immediate translational relevance and overcome the limited penetration depth of fluorescence optical imaging [65]. Furthermore, numerous studies have investigated the tumour-targeted approach for fluorescence image-guided surgery (such as folate receptor α, HER2, VEGF, osteonectin etc.), in addition to targeted drug delivery with promising results [13,66-69]. Thus, it would be interesting to further explore the application of CD24 conjugated to more NIR-shifted fluorophores in real-time intraoperative identification to improve the detection and surgical resection of malignant metastatic lesions [14,70].

In conclusion, we have identified CD24 as an imaging biomarker of HGSOC. Application of a monoclonal antibody targeting CD24 labelled with the near-infrared fluorophore Alexa Fluor 680 (CD24-AF680) was demonstrated to functionally visualise the pathogenesis of several preclinical models of HGSOC, including previously undescribed HGSOC cell line xenograft models of OV-90^{luc+}, Caov-3^{luc+}, and HGSOC PDXs (n = 7). CD24-AF680 neither affected cell viability *in vitro*, nor disease dissemination *in vivo*. Comparative optical imaging of cell line xenografts expressing bioluminescent reporters illustrated that FLI of CD24-AF680 permitted earlier disease contrast in peritoneal regions than BLI. CD24-AF680 could be used to image HGSOC therapeutic efficacy of new targeted therapy and immunotherapy combination strategies in orthotopic humanised HGSOC mice *in vivo*, and engraftment in PDX models with low CD24 expression and other peritoneally disseminating anaplastic cancers. Finally, CD24-AF680 allowed for real-time intraoperative identification of both the primary tumour and metastases in EOC xenografts. The findings demonstrate the successful use of an antibody mediated fluorescence imaging protocol of HGSOC PDX models that may be translatable as a clinical theranostics.

Declaration of Competing Interest

The authors declare that they have no conflicts of interest.

Acknowledgments

The authors acknowledge the technical support by Lars Herfindal, Mireia Safont Bendik Nordanger and Ingeborg Winge. Parts of this project were conducted with assistance of Tina Fonnes and Camilla Krakstad from the Bergen gynaecologic Cancer Research group, UiB. The authors acknowledge the Flow Cytometry Core Facility and the Molecular Imaging Center (MIC), University of Bergen. Further, the authors acknowledge the support from the MARIE SKLODOSWKA-CURIE ACTION (proposal number 675743; acronym ISPIC) carried out within the H2020 program MSCA-ITN funded by the EU.

Funding sources

Katrin Kleinmanns, Shamundeeswari Anandan and Vibeke Fosse are part of the project "Image-Guided surgery and Personalised Post-operative Immunotherapy to Improving Cancer Outcome" (ISPIC) funded though the H2020 program MSCA-ITN under grant agreement number 675743. Katharina Bischof and Ida Karlsen are supported by Helse Vest RHF and Helse Bergen HF (project numbers 911809, 911852). Mihaela Popa is employed by KinN Therapeutics. Financial support from Helse Vest RHF and Helse Bergen HF (project numbers 911809, 911852, 912171, 240222, HV1269) as well as The Norwegian Cancer Society (182735) and The Research Council of Norway through its Centers of excellence funding scheme (project number 223250, 262652) has been granted to Line Bjørge, Bjørn T. Gjertsen, Lars A. Akslen and Emmet McCormack. The Funding sources had no involvement in the writing, collection, analysis, interpretation or submission of the study and full access to the study data was provided.

Author's Contributions

Literature search: E. McCormack, L. Bjørge, K. Bischof, K. Kleinmanns

Study design: E. McCormack, L. Bjørge, BT. Gjertsen, K. Bischof, K. Kleinmanns

Development of methodology: E. McCormack, K. Kleinmanns, K. Bischof

Data collection (*in vitro* data, animal experiments, patient data): K. Bischof, K. Kleinmanns, S. Anandan, M. Popa, LA. Akslen, I. Karlsen, V. Fosse

Figures: K. Kleinmanns

Data analysis and interpretation of data (statistical analysis): K. Kleinmanns, K. Bischof, LA. Akslen, M. Popa

Writing, review and/or revision of the manuscript: K. Bischof, K. Kleinmanns, E. McCormack, L. Bjørge, LA. Akslen, V. Fosse

Study supervision: E. McCormack, L. Bjørge

All authors read and approved the final version of the manuscript.

Supplementary materials

Supplementary material associated with this article can be found in the online version at doi:10.1016/j.ebiom.2020.102782.

of x400 mm (e) Monthly longitudinally fluorescence imaging illustrates linear increase in mean fluorescence intensity in orthotopic PDX models. IHC CD24 staining (scale bars: original magnification of x400 mm) and *ex vivo* imaging (scale bar 1 cm) confirmed high CD24 expression and tumour growth in the ovary and liver (staining index 9 and 6, respectively; scale: negative 0 – 9 high). Images are presented with the minimum to maximum fluorescence intensity for each mouse (p/s/cm^2/sr). GI = gastrointestinal tract.

References

[1] Lheureux S, Braunstein M, Oza AM. Epithelial ovarian cancer: evolution of management in the era of precision medicine. CA Cancer J Clin 2019;393 (10177):1240–53.
[2] Morgan Jr. RJ, Alvarez RD, Armstrong DK, et al. Epithelial ovarian cancer. J Natl Compr Canc Netw 2011;9(1):82–113.
[3] Vergote I, du Bois A, Amant F, Heitz F, Leunen K, Harter P. Neoadjuvant chemotherapy in advanced ovarian cancer: on what do we agree and disagree? Gynecol Oncol 2013;128(1):6–11.
[4] du Bois A, Reuss A, Pujade-Lauraine E, Harter P, Ray-Coquard I, Pfisterer J. Role of surgical outcome as prognostic factor in advanced epithelial ovarian cancer: a combined exploratory analysis of 3 prospectively randomized phase 3 multicenter trials: by the arbeitsgemeinschaft gynaekologische onkologie studiengruppe ovarialkarzinom (AGO-OVAR) and the groupe d'investigateurs nationaux Pour les Etudes des cancers de l'Ovaire (GINECO). Cancer 2009;115(6):1234–44.
[5] Karam A, Ledermann JA, Kim JW, et al. Fifth ovarian cancer consensus conference of the gynecologic cancer inter-group: first-line interventions. Ann Oncol 2017;28(4):711–7.
[6] Fang Y, McGrail DJ, Sun C, et al. Sequential therapy with PARP and WEE1 inhibitors minimizes toxicity while maintaining efficacy. Cancer Cell 2019;35(6):851–67 e7.
[7] Yi J, Liu C, Tao Z, et al. MYC status as a determinant of synergistic response to Olaparib and Palbociclib in ovarian cancer. EBioMedicine 2019;43:225–37.
[8] van Scheltinga AGT, van Dam GM, Nagengast WB, et al. Intraoperative near-infrared fluorescence tumor imaging with vascular endothelial growth factor and human epidermal growth factor receptor 2 targeting antibodies. J Nucl Med 2011;52(11):1778–85.
[9] Debie P, Vanhoeij M, Poortmans N, et al. Improved debulking of peritoneal tumor implants by near-infrared fluorescent nanobody image guidance in an experimental mouse model. Mol Imag Biol 2018;20(3):361–7.
[10] Mahalingam SM, Kularatne SA, Myers CH, et al. Evaluation of novel tumor-targeted near-infrared probe for fluorescence-guided surgery of cancer. J Med Chem 2018;61(21):9637–46.
[11] Coustets M, Ladurantie C, Bellard E, et al. Development of a near infrared protein nanoprobe targeting Thomsen-Friedenreich antigen for intraoperative detection of submillimeter nodules in an ovarian peritoneal carcinomatosis mouse model. Biomaterials 2020:119908.
[12] van Driel PB, Boonstra MC, Prevoo HA, et al. EpCAM as multi-tumour target for near-infrared fluorescence guided surgery. BMC Cancer 2016;16(1):884.
[13] van Dam GM, Themelis G, Crane LM, et al. Intraoperative tumor-specific fluorescence imaging in ovarian cancer by folate receptor-alpha targeting: first in-human results. Nat Med 2011;17(10):1315–9.
[14] Randall LM, Wenham RM, Low PS, Dowdy SC, Tanyi JL. A phase II, multicenter, open-label trial of OTL38 injection for the intra-operative imaging of folate receptor-alpha positive ovarian cancer. Gynecol Oncol 2019(19):31396. S0090-8258-4.
[15] Bowtell DD, Bohm S, Ahmed AA, et al. Rethinking ovarian cancer II: reducing mortality from high-grade serous ovarian cancer. Nat Rev Cancer 2015;15(11):668–79.
[16] Gengenbacher N, Singhal M, Augustin HG. Preclinical mouse solid tumour models: status quo, challenges and perspectives. Nat Rev Cancer 2017;17(12):751.
[17] Kuhn E, Tisato V, Rimondi E, Secchiero P. Current preclinical models of ovarian cancer. J Carcinog Mutagen 2015;6(2):220.
[18] Sherman−Baust CA, Kuhn E, Valle BL, et al. A genetically engineered ovarian cancer mouse model based on fallopian tube transformation mimics human high−grade serous carcinoma development. J Pathol 2014;233(3):228–37.
[19] Helland O, Popa M, Vintermyr OK, et al. First in-mouse development and application of a surgically relevant xenograft model of ovarian carcinoma. PLoS ONE 2014;9(3):e89527.
[20] Domcke S, Sinha R, Levine DA, Sander C, Schultz N. Evaluating cell lines as tumour models by comparison of genomic profiles. Nat Commun 2013;4:2126.
[21] Mitra AK, Davis DA, Tomar S, et al. *In vivo* tumor growth of high-grade serous ovarian cancer cell lines. Gynecol Oncol 2015;138(2):372–7.
[22] Weroha SJ, Becker MA, Enderica-Gonzalez S, et al. Tumorgrafts as *in vivo* surrogates for women with ovarian cancer. Clin Cancer Res 2014;20(5):1288–97.
[23] Topp MD, Hartley L, Cook M, et al. Molecular correlates of platinum response in human high-grade serous ovarian cancer patient-derived xenografts. Mol Oncol 2014;8(3):656–68.
[24] Hidalgo M, Amant F, Biankin AV, et al. Patient-derived xenograft models: an emerging platform for translational cancer research. Cancer Discov 2014;4 (9):998–1013.
[25] Wakefield C, Doolan E, Fardell J, et al. The Avatar Acceptability Study: survivor, Parent and Community Willingness to Use Patient-Derived Xenografts to Personalize Cancer Care. EBioMedicine 2018;37:205–13.
[26] George E, Kim H, Krepler C, et al. A patient-derived-xenograft platform to study BRCA-deficient ovarian cancers. JCI Insight 2017;2(1):e89760.
[27] Scott CL, Becker MA, Haluska P, Samimi G. Patient-derived xenograft models to improve targeted therapy in epithelial ovarian cancer treatment. Front Oncol 2013;3:295.
[28] Shaw TJ, Senterman MK, Dawson K, Crane CA, Vanderhyden BC. Characterization of intraperitoneal, orthotopic, and metastatic xenograft models of human ovarian cancer. Mol Ther 2004;10(6):1032–42.
[29] Haldorsen IS, Popa M, Fonnes T, et al. Multimodal Imaging of orthotopic mouse model of endometrial carcinoma. PLoS ONE 2015;10(8):e0135220.
[30] Liu JF, Palakurthi S, Zeng Q, et al. Establishment of patient-derived tumor xenograft models of epithelial ovarian cancer for preclinical evaluation of novel therapeutics. Clin Cancer Res 2017;23(5):1263–73.
[31] McCormack E, Micklem DR, Pindard LE, et al. *In vivo* optical imaging of acute myeloid leukemia by green fluorescent protein: time-domain autofluorescence decoupling, fluorophore quantification, and localization. Mol Imag 2007;6 (3):193–204.
[32] McCormack E, Haaland I, Venas G, et al. Synergistic induction of p53 mediated apoptosis by valproic acid and nutlin-3 in acute myeloid leukemia. Leukemia 2012;26(5):910–7.
[33] Hilderbrand SA, Weissleder R. Near-infrared fluorescence: application to *in vivo* molecular imaging. Curr Opin Chem Biol 2010;14(1):71–9.
[34] Wang P, Fan Y, Lu L, et al. NIR-II nanoprobes in-vivo assembly to improve image-guided surgery for metastatic ovarian cancer. Nat Commun 2018;9(1):2898.
[35] He H, Tu X, Zhang J, et al. A novel antibody targeting CD24 and hepatocellular carcinoma *in vivo* by near-infrared fluorescence imaging. Immunobiology 2015;220 (12):1328–36.
[36] McCormack E, Mujic M, Osdal T, Bruserud O, Gjertsen BT. Multiplexed mAbs: a new strategy in preclinical time-domain imaging of acute myeloid leukemia. Blood 2013;121(7):e34–42.
[37] Cilliers C, Nessler I, Christodolu N, Thurber GM. Tracking antibody distribution with near-infrared fluorescent dyes: impact of dye structure and degree of labeling on plasma clearance. Mol Pharm 2017;14(5):1623–33.
[38] Zhang L, Bhatnagar S, Deschenes E, Thurber GM. Mechanistic and quantitative insight into cell surface targeted molecular imaging agent design. Sci Rep 2016;6 (1):1–13.
[39] Lorens JB, Jang Y, Rossi AB, Payan DG, Bogenberger JM. Optimization of regulated LTR-mediated expression. Virology 2000;272(1):7–15.
[40] McCormack E, Micklem DR, Pindard L-E, et al. *In vivo* optical imaging of acute myeloid leukemia by green fluorescent protein: time-domain autofluorescence decoupling, fluorophore quantification, and localization. Mol Imag 2007;6 (3):7290.2007. 00016.
[41] McCormack E, Mujić M, Osdal T, Bruserud Ø, Gjertsen BT. Multiplexed mAbs: a new strategy in preclinical time-domain imaging of acute myeloid leukemia. Blood 2013;121(7):e34–42.
[42] Poli A, Wang J, Domingues O, et al. Targeting glioblastoma with NK cells and mAb against NG2/CSPG4 prolongs animal survival. Oncotarget 2013;4(9):1527.
[43] Leitch C, Osdal T, Andresen V, et al. Hydroxyurea synergizes with valproic acid in wild-type p53 acute myeloid leukaemia. Oncotarget 2016;7(7):8105.
[44] Barkal AA, Brewer RE, Markovic M, et al. CD24 signalling through macrophage Siglec-10 is a target for cancer immunotherapy. Nature 2019;572(7769):392–6.
[45] Lee J-H, Kim S-H, Lee E-S, Kim Y-S. CD24 overexpression in cancer development and progression: a meta-analysis. Oncol Rep 2009;22(5):1149–56.
[46] Sagiv E, Starr A, Rozovski U, et al. Targeting CD24 for treatment of colorectal and pancreatic cancer by monoclonal antibodies or small interfering RNA. Cancer Res 2008;68(8):2803–12.
[47] Kristiansen G, Denkert C, Schlüns K, Dahl E, Pilarsky C, Hauptmann S. CD24 is expressed in ovarian cancer and is a new independent prognostic marker of patient survival. Am J Pathol 2002;161(4):1215–21.
[48] Peterson VM, Castro CM, Chung J, et al. Ascites analysis by a microfluidic chip allows tumor-cell profiling. Proc Natl Acad Sci U S A 2013;110(51):E4978–86.
[49] Choi YL, Kim SH, Shin YK, et al. Cytoplasmic CD24 expression in advanced ovarian serous borderline tumors. Gynecol Oncol 2005;97(2):379–86.
[50] Davidson B. CD24 is highly useful in differentiating high-grade serous carcinoma from benign and malignant mesothelial cells. Hum Pathol 2016;58:123–7.
[51] Nakamura K, Terai Y, Tanabe A, et al. CD24 expression is a marker for predicting clinical outcome and regulates the epithelial-mesenchymal transition in ovarian cancer via both the Akt and ERK pathways. Oncol Rep 2017;37(6):3189–200.
[52] Overdevest JB, Thomas S, Kristiansen G, Hansel DE, Smith SC, Theodorescu D. CD24 offers a therapeutic target for control of bladder cancer metastasis based on a requirement for lung colonization. Cancer Res 2011;71(11):3802–11.
[53] Anglesio MS, Wiegand KC, Melnyk N, et al. Type-specific cell line models for type-specific ovarian cancer research. PLoS ONE 2013;8(9):e72162.
[54] Beaufort CM, Helmijr JC, Piskorz AM, et al. Ovarian cancer cell line panel (OCCP): clinical importance of *in vitro* morphological subtypes. PLoS ONE 2014;9(9): e103988.
[55] Gao H, Korn JM, Ferretti S, et al. High-throughput screening using patient-derived tumor xenografts to predict clinical trial drug response. Nat Med 2015;21 (11):1318–25.
[56] Kim H, Kang H, Shim H, et al. Co-clinical trials demonstrate predictive biomarkers for dovitinib, an FGFR inhibitor, in lung squamous cell carcinoma. Ann Oncol 2017;28(6):1250–9.
[57] Rehemtulla A, Stegman LD, Cardozo SJ, et al. Rapid and quantitative assessment of cancer treatment response using *in vivo* bioluminescence imaging. Neoplasia 2000;2(6):491–5.
[58] Joshi BP, Wang TD. Targeted Optical Imaging Agents in Cancer: focus on Clinical Applications. Contrast Media Mol Imag 2018;2018(2015237):19.
[59] Hernot S, van Manen L, Debie P, Mieog JSD, Vahrmeijer AL. Latest developments in molecular tracers for fluorescence image-guided cancer surgery. Lancet Oncol 2019;20(7):e354–e67.
[60] Nagaya T, Nakamura YA, Choyke PL, Kobayashi H. Fluorescence-guided surgery. Front Oncol 2017;7:314.
[61] Ceppi L, Bardhan NM, Na Y, et al. Real-time single-walled carbon nanotube-based fluorescence imaging improves survival after Debulking surgery in an ovarian cancer model. ACS Nano 2019;13(5):5356–65.

[62] Asanuma D, Sakabe M, Kamiya M, et al. Sensitive β-galactosidase-targeting fluorescence probe for visualizing small peritoneal metastatic tumours *in vivo*. Nat Commun 2015;6(1):1–7.
[63] Salnikov AV, Bretz NP, Perne C, et al. Antibody targeting of CD24 efficiently retards growth and influences cytokine milieu in experimental carcinomas. Br J Cancer 2013;108(7):1449–59.
[64] Klapdor R, Wang S, Morgan M, et al. Characterization of a novel third-generation Anti-CD24-CAR against ovarian cancer. Int J Mol Sci 2019;20(3).
[65] Derks YH, Löwik DW, Sedelaar JM, et al. PSMA-targeting agents for radio-and fluorescence-guided prostate cancer surgery. Theranostics 2019;9(23):6824.
[66] Liu TW, Stewart JM, MacDonald TD, et al. Biologically-targeted detection of primary and micro-metastatic ovarian cancer. Theranostics 2013;3(6):420.
[67] Maurer AH, Elsinga P, Fanti S, Nguyen B, Oyen WJ, Weber WA. Imaging the folate receptor on cancer cells with 99mTc-etarfolatide: properties, clinical use, and future potential of folate receptor imaging. J Nucl Med 2014;55(5):701–4.
[68] Sasaki Y, Miwa K, Yamashita K, et al. A phase I study of farletuzumab, a humanized anti-folate receptor α monoclonal antibody, in patients with solid tumors. Invest New Drugs 2015;33(2):332–40.
[69] Tummers QR, Hoogstins CE, Gaarenstroom KN, et al. Intraoperative imaging of folate receptor alpha positive ovarian and breast cancer using the tumor specific agent EC17. Oncotarget 2016;7(22):32144–55.
[70] Hoogstins CE, Tummers QR, Gaarenstroom KN, et al. A novel tumor-specific agent for intraoperative near-infrared fluorescence imaging: a translational study in healthy volunteers and patients with ovarian cancer. Clin Cancer Res 2016;22(12):2929–38.